

Sediment Thickness of the Contiguous United States from Teleseismic Receiver Functions

OPEN  ACCESS

Augustin Marignier^{*1} , Caroline M. Eakin¹ , and Meghan S. Miller¹ 

Abstract

Sediment thickness is a crucial measure for many seismic studies. The slow seismic velocities associated with thick sedimentary sequences can be problematic when inverting for regional tomographic images of the crust and upper-mantle structure, and is an essential piece of information for better constraining ground-motion models as sediments can amplify shaking. Yet there is currently no map of sediment thickness across the contiguous United States that is not a combination of smaller regional studies with potentially inconsistent methodologies. In this work, we measure the delay time of *P* to *S* conversions at the sediment–basement interface from a set of teleseismic receiver functions and demonstrate the geographical correlation with known sedimentary provinces. From this, we produce two maps of sediment thickness, using (1) a borehole-derived empirical relation and (2) the mean velocity in the upper 5 km of a tomographic model. Although the former is likely an underestimate, the latter is an excellent first-order representation of sediment thickness across the United States.

Cite this article as Marignier, A., C. M. Eakin, and M. S. Miller (2025). Sediment Thickness of the Contiguous United States from Teleseismic Receiver Functions, *Seismol. Res. Lett.* **XX**, 1–9, doi: 10.1785/0220250077.

[Supplemental Material](#)

Introduction

Given the well-known effects of sedimentary basins on ground motion (e.g., Molnar *et al.*, 2014; Wirth *et al.*, 2019), it is crucial to understand the structure and thicknesses of these basins for accurate ground-motion models. In the United States, ground-motion models typically account for the sediment thickness by picking the depth of the 1.0 km s^{-1} and 2.5 km s^{-1} shear-wave velocity contour from a tomographic model (e.g., Abrahamson *et al.*, 2014; Boore *et al.*, 2014; Campbell and Bozorgnia, 2014) or the time-averaged velocity in the upper 30 m of the crust (V_{S30} , e.g., Petersen *et al.*, 2020). Some recent work has gone into looking more closely at sedimentary basins and their effect on ground-motion predictions, which tend to focus on seismically active localities, such as basins in metropolitan Los Angeles (e.g., Ghose *et al.*, 2023). In the 2018 update to the U.S. National Seismic Hazard Model (Petersen *et al.*, 2020), basin depth was introduced for the first time for basins in the western United States. To continue this work for other parts of the country, Boyd *et al.* (2024) developed a new sediment thickness model for the Atlantic and Gulf Coastal Plains, incorporating digitized maps, hydrogeological reports, and well data to identify the base of the Cretaceous and Mesozoic sediments.

A sediment thickness map across the entire United States based on a consistent methodology may therefore benefit future updates of the national seismic hazard model. Currently, the most commonly utilized map of sediment thickness for

North America is that of Mooney and Kaban (2010) (hereafter referred to as MK10), which is primarily based on a compilation of hydrocarbon resource exploration studies. This map has been used for studies including seismic imaging of crustal and upper-mantle structures (e.g., Shen *et al.*, 2012, 2013; Ekström, 2014; Shen and Ritzwoller, 2016) and is used to fill in gaps in local sediment thickness models (e.g., Boyd *et al.*, 2024). Although this map provides a good overview of the main sedimentary provinces because it is based on regional and local compilations of particular basins, some regions are more detailed while others are lacking in information (Fig. 1). For example, a narrow band of no sediments along the northwestern boundary of the Atlantic plain appears to be the result of a gap in the original map from Frezon *et al.* (1983). Sediment thickness maps constrained from select regional models may therefore lead to inconsistencies for continent-wide interpretations.

The seismic structure of the United States has been extensively studied, with EarthScope's Transportable Array network

1. Research School of Earth Sciences, Australian National University, Acton, Australian Capital Territory, Australia,  <https://orcid.org/0000-0001-6778-1399> (AM);  <https://orcid.org/0000-0001-9187-3138> (CME);  <https://orcid.org/0000-0001-5494-2296> (MSM)

*Corresponding author: augustin.marignier@anu.edu.au

Copyright © 2025. The Authors. This is an open access article distributed under the terms of the CC-BY license, which permits unrestricted use, distribution, and reproduction in any medium, provided the original work is properly cited.

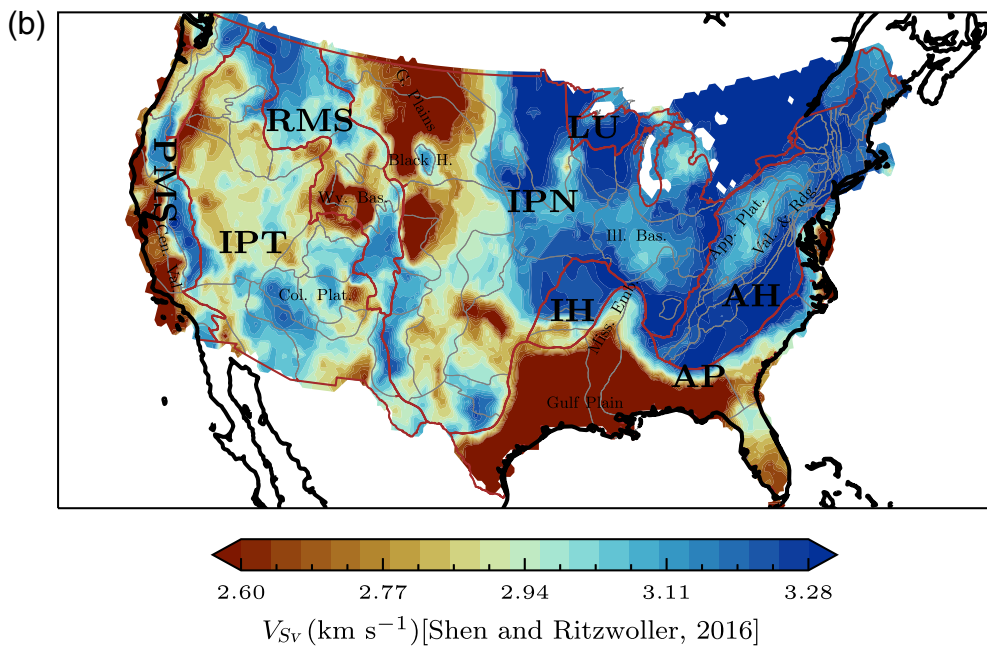
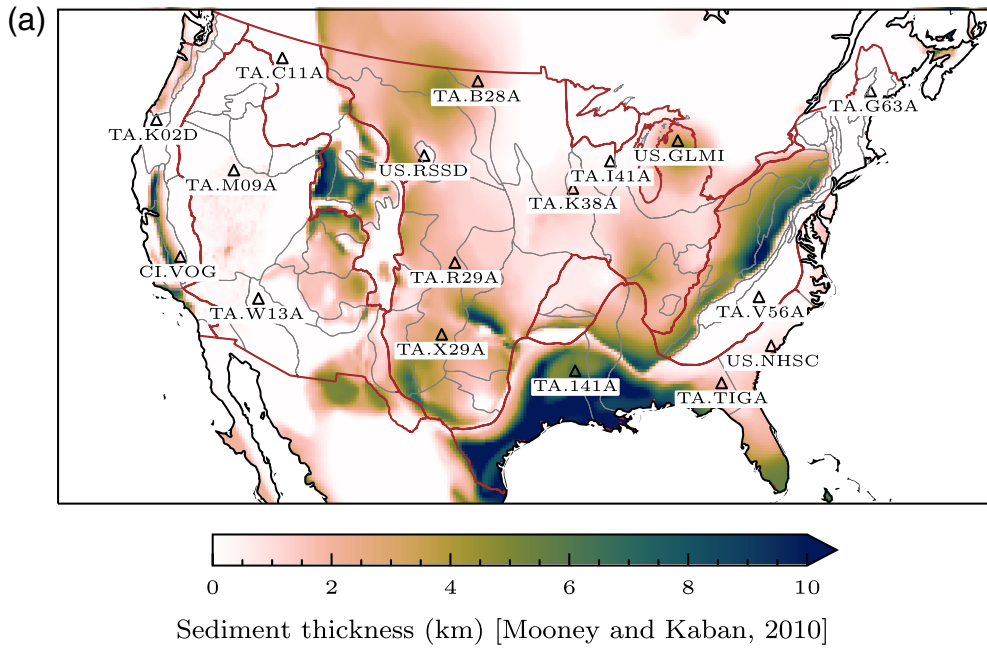


Figure 1. (a) Sediment thickness estimated by MK10. The triangles indicate the locations of example seismic stations for which receiver functions (RFs) are shown in Figure 2. (b) The mean shear velocity (V_{Sv}) of the top 5 km of the tomography model of Shen and Ritzwoller (2016). The brown and gray lines delineate the physiographic divisions and sections, respectively, of Fenneman and Johnson (1946). AH, Appalachian Highlands; AP, Atlantic Plain; IH, Interior Highlands; IPN, Interior Plains; IPT, Intermontane Plateaus; LU, Laurentian Upland; PMS, Pacific Mountain System; RMS, Rocky Mountain System. The color version of this figure is available only in the electronic edition.

(Incorporated Research Institutions for Seismology [IRIS] Transportable Array, 2003). A range of seismic observables have been used, including body-wave arrivals and surface-wave dispersion and amplitudes, to build regional and continent-wide images (e.g., Moschetti *et al.*, 2007; Lin *et al.*, 2008; Liu *et al.*, 2011; Levander and Miller, 2012; Chai *et al.*, 2015; Schmandt

et al., 2015; Shen and Ritzwoller, 2016; Chai *et al.*, 2022; Sturgeon *et al.*, 2023), usually targeting the crust and upper mantle, with the shallow sediment layer being incorporated into the crustal component. Shen and Ritzwoller (2016) inverted explicitly for the shear velocity at the top and bottom of a sediment layer and its thickness, with the thickness parameterized as a perturbation around the MK10 model; however, this result was not shown or discussed explicitly in their article nor made available in the model files. Taking the upper 5 km of the model, some discrepancies with MK10 can be seen (Fig. 1). For example, in some areas, slow velocities in California's Central Valley extend all the way to the coast, but thick sediments are contained mainly within the valley. In the northern Great Plains, slow velocities in the tomography are more widespread than thick sediments are in the sediment thickness map. The global model CRUST1.0 (Laske *et al.*, 2012) and part of its constituent data (Laske, 1997) are often used as reference points for sediment thickness; however, given the relatively low resolution of $1^\circ \times 1^\circ$ cells, they lack sufficient detail for regional and local studies.

This study aims to produce a continent-wide sediment thickness map, using a new simple empirical approach (Agrawal *et al.*, 2022; Marignier *et al.*, 2024) based on a direct measurement from teleseismic receiver functions (RFs) without the need for inversion. This empirical relation was derived using Australian RF and borehole data, and part of our objective in this study is to assess whether the relation is generalizable to other regions. In addition, we exploit the excellent seismic station coverage that underpins previously published RFs and

seismic tomography models to then predict sediment thickness across the conterminous United States.

Method

RFs computed from teleseismic events indicate the arrival time of seismic waves converted from P to S at seismic discontinuities such as the Moho and their later multiples. They have been used extensively to study the crust and upper-mantle structure of many regions, including the United States. Recent work has started to look at the use of RFs to look directly at the sediment layer on continents (e.g., Cunningham and Lekic, 2020; Agrawal *et al.*, 2022; Deng *et al.*, 2023; Marignier *et al.*, 2024) and the seafloor (e.g., Chichester *et al.*, 2020; Kim *et al.*, 2023). In previous work (Agrawal *et al.*, 2022; Marignier *et al.*, 2024), we have shown that the delay time of the first positive peak on a radial RF is highly sensitive to the thickness of sediments. This is based on the assumption that in the presence of sediments, the first arrival on the radial RF can be that of the P wave converted to S at the interface of sediment and the crystalline basement, rather than the direct P . A similar observation has been made in two Californian radial RFs (Berg *et al.*, 2021; Li *et al.*, 2022). On the other hand, the P to S conversion at the sediment–basement interface has been observed just after the direct P in other RF studies in sedimentary basins in California, Texas, and the south-central United States where it has been noted that the frequency content of the RFs and basin depth affect the ability to distinguish these phases (Liu *et al.*, 2018; Wang *et al.*, 2021; Sadler and Pulliam, 2023, 2025). What we call “sediment” or “sedimentary rock” throughout this work is the largest shallow impedance contrast, which has been shown in previous work to correlate with the sediment–basement interface (Agrawal *et al.*, 2022; Marignier *et al.*, 2024). Our method provides no velocity information, unlike alternatives such as that proposed by Yeck *et al.* (2013), which is based on $H - \kappa$ stacking, and thus we have no constraint on rock type. As discussed in previous work (e.g., Marignier *et al.*, 2024), this leaves open the possibility that the interface we are detecting is intrasedimentary. The sequential $H - \kappa$ approach (Yeck *et al.*, 2013) also makes use of multiples within the sediment layer, arguably improving robustness. This, however, means that the multiples need to be present, and accurately picked or modeled in the RF, which limits regions of applicability to those where the sediments are sufficiently thick or where higher frequency RFs are considered. Our method, while arguably crude, is based on a single pick per RF, which is available even in thin sediments, and bypasses the need for a grid search or other inversion method, meaning we can obtain an estimate of sediment thickness continent-wide quickly.

The time of our phase of interest, t_{Ps_b} , is related to the thickness of the sediment layer, D , and the shear and compressional velocities of the sediments, V_S and V_P , by

$$t_{Ps_b} = \int_0^D \left(\frac{1}{V_S(z)} - \frac{1}{V_P(z)} \right) dz, \quad (1)$$

in which z denotes depth. This assumes vertical incidence of the P phase, an assumption we carry throughout this work because it has been shown to introduce negligible error compared to observational uncertainties (Cunningham and Lekic, 2020). Using RFs and boreholes in Australia, we obtained the following empirical relationship (Marignier *et al.*, 2024) between t_{Ps_b} and D for Phanerozoic sedimentary rocks,

$$D = 1369.64 t_{Ps_b}^2 - 545.52 t_{Ps_b} + 382.62, \quad (2)$$

in which D is in meters and t_{Ps_b} is in seconds. This equation is constructed based on sediments of a wide range of ages spanning the entire Australian continent, and is thus potentially applicable in other continental regions. This study acts as a first test of the generalizability of the empirical relation. With the dense array of seismic stations deployed across the United States and extensive seismic tomography work done in the region, we can now combine the t_{Ps_b} time as measured from RFs with the V_S derived from tomography to solve equation (1) for D and obtain a continent-wide sediment thickness map.

Seismic observations

We use a precompiled data set of seismic RFs (IRIS DMC, 2010) generated using the automated process of Crotwell and Owens (2005). With this data set we obtain radial RFs from the networks TA, CI, BK, US, and AZ (see Open Research section). Notable gaps in this RF data set exist in the southernmost part of the Gulf Coastal Plains and in the interior of the California Central Valley, where thick sediments are expected (Fig. 1a). We suspect that the thick sediments in these regions complicated the character of the RFs in such a way that the automated procedure could not produce a reliable result, and thus did not pass quality control. We repeated the procedure of Crotwell and Owens (2005), minus the quality control, for 10 select stations from the BK network to fill the gap in the Central Valley, using events dating back to 2005. RFs at each station are stacked and processed according to Marignier *et al.* (2024). Representative samples of the final radial RFs are shown in Figure 2. Following an automated process for measuring the t_{Ps_b} time (Marignier *et al.*, 2024) and some manual corrections for 30 anomalous stations (Supporting Information Fig. S1 and Table S1, available in the supplemental material to this article), we obtain measurements at 1835 stations across the conterminous United States (Fig. 3).

The t_{Ps_b} times show consistent geographical patterns and a clear spatial correlation with the expected distribution of sedimentary basins. Point-by-point correlations between the maps in Figures 1 and 3 are shown in Figure S2. The physiographic regions are well delineated to a first order. Large delays (black circles, >1 s) mark the interior and northwestern extent of the Atlantic Plain, continuing up the eastern seaboard. We also see these large delays (>1 s) in the northwest of the Interior Plains

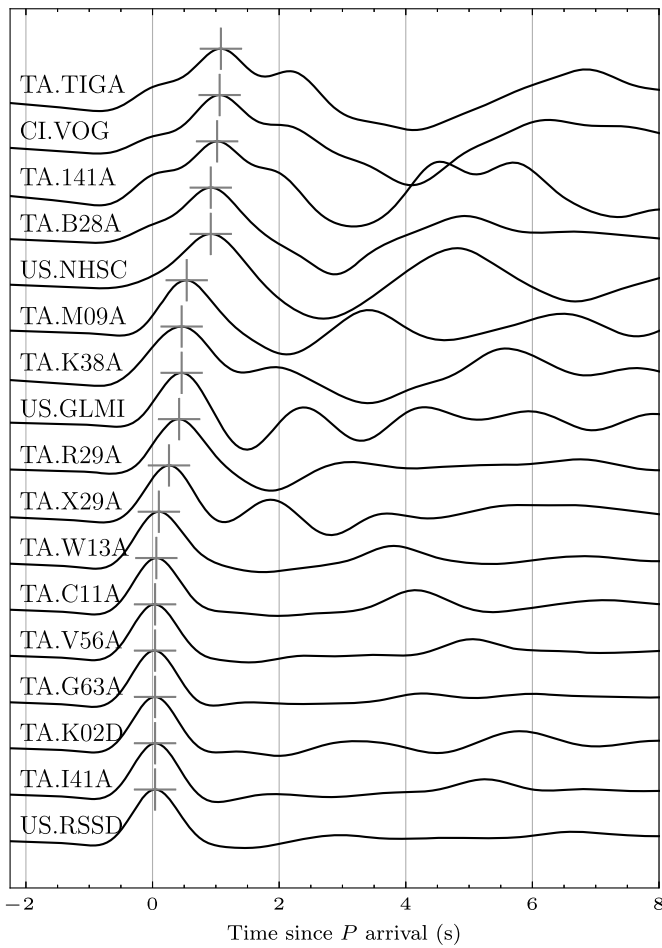


Figure 2. Stacked radial RFs (0.1–1.0 Hz) presented for a representative sample of seismic stations (Fig. 1), produced by the automated method (Crotwell and Owens, 2005) and found in the EarthScope automated receiver survey (EARS) database, sorted by t_{Ps_b} delay time. The gray crosses mark the arrival of the Ps_b phase as found in the method described in Agrawal et al. (2022). At least 10 events are used for each stack.

and progressively shorter delays (~ 0.5 s) extending south toward Texas. This largely corresponds with the location of the western Interior basin (Miall et al., 2008). A clear drop in t_{Ps_b} (from >1 to <0.2 s) crossing over into the Rocky Mountain System to the west from the Interior Plains is also observed. Moderate delays (~ 0.1 – 0.4 s, i.e., orange colors) are observed in the northwest of the Appalachian Highlands province, corresponding to the Appalachian basin (Ettensohn, 2008). In the Basin and Range, we see a full range of t_{Ps_b} times, reflective of the complex faulted topography of alternating horst and grabens across the region. Stations in the Central Valley show a generally larger t_{Ps_b} (~ 0.5 s) than in the rest of the Coast Ranges and the Sierra Nevada.

Sediment thickness predictions

To obtain sediment thickness from the t_{Ps_b} times, we utilize the tomographic model of Shen and Ritzwoller (2016). This model

is chosen because it is based on the joint inversion of RFs and surface-wave dispersion and amplitude data, and it provides a 3D shear velocity model of the crust and upper mantle for the conterminous United States. We use the mean shear velocity in the top 5 km of the model on a $0.25^\circ \times 0.25^\circ$ grid to represent the sediment shear velocity. Scaling the shear velocity using an empirical relation to obtain compressional velocity (Brocher, 2005, his equation 9), we then solve equation (1) for sediment thickness. Assuming a constant velocity with depth in the sedimentary layer results in a simple linear scaling of t_{Ps_b} ,

$$D = \frac{V_p V_s}{V_s - V_p} t_{Ps_b}, \quad (3)$$

in contrast to the more complex quadratic relationship found in Marignier et al. (2024). We compare the sediment thickness predictions using the tomography model with those using the empirical relationship in Figure 4. In basin studies for ground-motion models, the sediment thickness is typically taken to be the $v_s = 1 \text{ km s}^{-1}$ or $v_s = 3 \text{ km s}^{-1}$ contour (e.g., Abrahamson et al., 2014; Boore et al., 2014; Campbell and Bozorgnia, 2014). We show maps of sediment thickness using these velocity values in Figure S5 for comparison; however, we note that the geographic pattern of sediment thickness does not change from what can be seen in the map of t_{Ps_b} times (Fig. 3) because the scaling factor in equation (3) is geographically constant in these cases.

As expected, the two estimates of sediment thickness show the same broad patterns, reflecting what was observed with the t_{Ps_b} times (Fig. 3). The clear delineations of the physiographic regions seen in the RF data remain in the sediment thickness predictions with some regional examples highlighted in Figure S6. The main difference between the estimates is the range of sediment thicknesses, with the estimate based on V_s from the tomographic model suggesting thicknesses several kilometers thicker than the empirical estimate. From the tomography, we obtain thicknesses greater than 6 km in the thickest regions, primarily the Gulf Coastal Plain and Western Interior basin. These are also the thickest areas using the empirical relationship, but with estimated total thicknesses less than 2 km.

Discussion

Evaluation of the method

Our t_{Ps_b} map is generally very well correlated with the tomographic model of Shen and Ritzwoller (2016), with larger values typically corresponding to regions of low shear-wave velocity in the upper 5 km (Fig. S3). This clear correlation further validates the t_{Ps_b} as a proxy for the shallowest sedimentary structure, while being much simpler to obtain than a tomographic image (i.e., without the need for inversion).

As previously discussed here and in recent work, a limitation of our method is the assumption that the phase we are picking on the radial RF is a result of the impedance contrast between

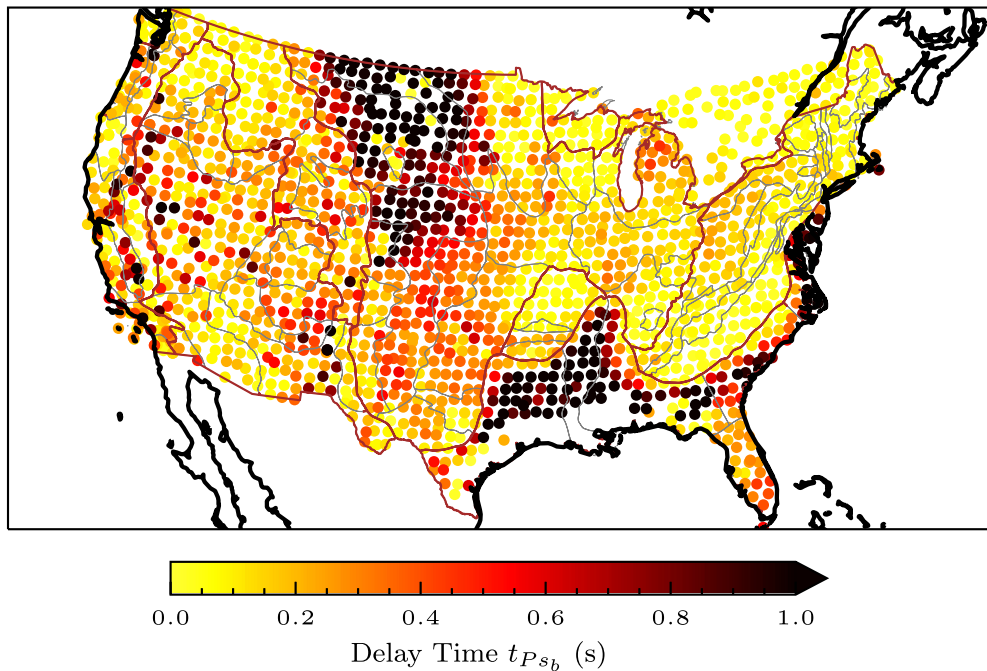


Figure 3. Times of the Ps_b phase relative to the direct P phase at individual seismic stations. The color version of this figure is available only in the electronic edition.

sediment and crystalline basement. Because the method has velocity constraint, we cannot be sure that there is no large intrasedimentary impedance contrast that is causing the delayed peak. Furthermore, at the frequencies we use the pick can be a mix of a Ps and a PPs phase (Yeck *et al.*, 2013; Cunningham and Lekic, 2020; Agrawal *et al.*, 2022), which can be distinguished at higher frequencies. Agrawal *et al.* (2022) showed that using a lower frequency does not produce a systematic underestimate or overestimate of the t_{Ps_b} delay time. A more sophisticated method such as that proposed by Yeck *et al.* (2013) is better suited for local studies of individual basins. Our approach, on the other hand, is more suited to a study of a large area where sedimentary basins may not even be present. We argue that the pattern of large delay times (Fig. 3) and broad spatial correlation with known sedimentary regions means that our pick, combined with a chosen velocity, can provide a good first-order estimate of sediment thickness for continental-scale surveys.

Clearly, the empirical relationship underestimates sediment thickness for the United States. The estimate based on tomography is considered to be more accurate here, although, as discussed further subsequently, the choice of velocity model is itself subject to limitations. This difference likely stems from the borehole database for Australia from which the empirical relationship was derived. Because of expense, the majority of boreholes are drilled in locations with little to no sediment cover, with very few boreholes drilled in Australia where the basement depth exceeds 3000 m. This suggests an upper limit to the applicability of the

empirical relationship, with thinner sedimentary cover better constrained (by more data) than when the sedimentary cover is many kilometers thick. Likely, the gradient of the relationship between t_{Ps_b} and sediment thickness is much steeper for thick sedimentary cover than could be resolved by the Australian borehole data. This is also supported by synthetic tests (Marignier *et al.*, 2024) in which the sediment thickness appears to become almost exponential with increasing t_{Ps_b} time. It will therefore be difficult to accurately predict the sediment thickness for larger t_{Ps_b} times with such an empirical relationship unless a borehole database with many deep drill holes becomes available.

Finally, the choice of velocity model used here to estimate sediment thickness from t_{Ps_b} is by no means necessarily the “correct” one. In this work, we have tested four different choices of velocity model, each of which has its own advantages and disadvantages. Using the mean shear wavespeed in the top 5 km from Shen and Ritzwoller (2016) means that in regions of thin sediments we are using a velocity value from the basement rock. This should in principle be counteracted by a small (if not 0) t_{Ps_b} -value, which is observed in Figure 4b. The empirical relationship (equation 2) was developed using Australian seismic and borehole data (Marignier *et al.*, 2024). Our objective in using it for the United States was to evaluate whether, given the range of geological ages and sediment thicknesses in Australia (Marignier *et al.*, 2024), the empirical relation generalizes to other continental regions. We have found that for the United States, it generally produces an underestimate of the sediment thickness. We further tested constant velocity models (Fig. S5) using velocity values typically contoured as the sediment basement. Although these produce reasonable results, they are just a constant scaling from the t_{Ps_b} map without any geographical variability. Ultimately, because we do not invert for velocity, the velocity remains a choice to be made by the researcher.

Comparison of sediment thickness maps

Comparing our results with the map from MK10, we note differences in the extent of some thick sediment regions, which are further outlined subsequently. Numerical values of our results refer to the tomography-based sediment thickness estimate (Fig. 4b).

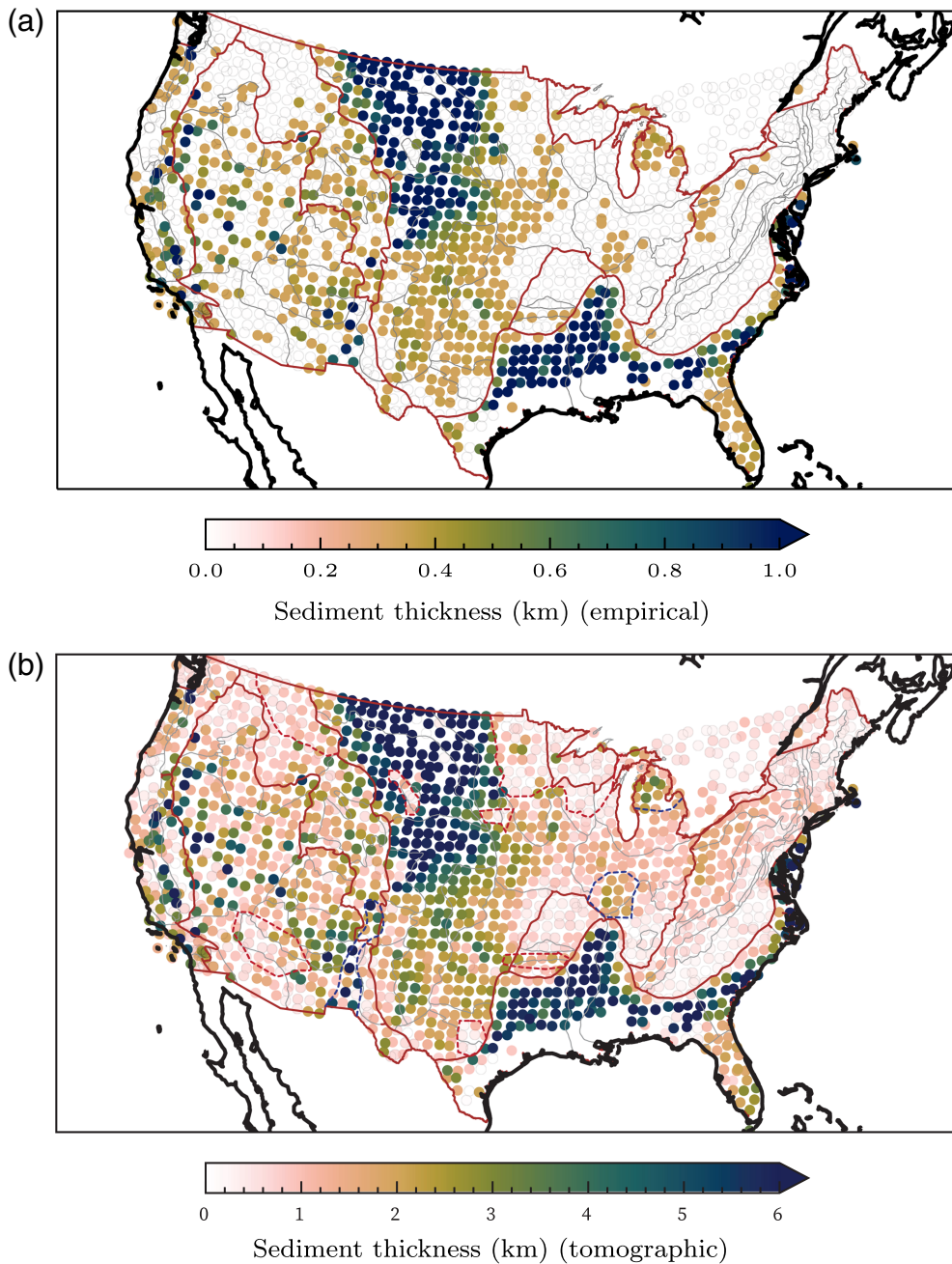


Figure 4. Sediment thickness at each seismic station derived using (a) the empirical relationship (equation 2) of Marignier et al. (2024), and (b) the shear-wave tomography model of Shen and Ritzwoller (2016), in combination with the t_{PS_b} delay times measured in this study. Note the difference in the color scales. Note the minimum in the empirical relationship at $(t_{PS_b}, D) = (0.2, 382.62)$ (equation 2). Stations below this minimum are shown simply by gray circles because the empirical relation is no longer consistent with a sediment compaction model (Marignier et al., 2024). Figure S4 shows an interpolation of (b). The red dashed lines correspond to outcropping basement areas from Marshak et al. (2016). The blue dashed lines highlight sedimentary features of interest not otherwise delineated mentioned in the text. From west to east these are the Rio Grande rift, Illinois basin, and Michigan's lower peninsula. The color version of this figure is available only in the electronic edition.

We estimate consistently thick sediments from the northern edge of the Gulf Coastal Plain and along the Mississippi embayment to Kentucky and into the Illinois basin. MK10 estimate the

results seems to correlate well with tomography (Fig. 1b), as well as with the location of the ancient Western Interior Seaway, which deposited thick shales and carbonates (Roberts and

thick sediments stopping south of the Gulf Plain edge and much thinner sediments in the north part of the embayment. Thicker sediments are observed along the Atlantic Coastal Plain in our analysis, particularly in southeastern Georgia and the Carolinas.

The central portion of North America is underlain by cratonic lithosphere, but the lithospheric structure was significantly deformed by tectonic processes throughout the Phanerozoic (Whitmeyer and Karlstrom, 2007). Regional scale intracratonic basins and local fault-and-fold zones are still active, most notably the seismically active mid-Continent rift (Whitmeyer and Karlstrom, 2007). The cratonic basins, such as the deep Illinois basin, have been studied by multiple groups, but most recently their structure has been interpreted with the OIINK experiment (Yang et al., 2017). The Illinois basin has been inferred to be as much as 7.5 km thick, which is estimated from the depth to the Great Unconformity (Domrois et al., 2015; Marshak et al., 2016). This is thicker than suggested by our results.

Sediments about 6 km thick in the northwest of the Interior Plains are more widespread in our thickness estimates than for MK10, where there are only two local regions of sediments of 5–6 km thick surrounded by thicknesses around 2 km, such as those basins adjacent to the Ozarks or where there are basement outcrops as presented by Marshak et al. (2016). The larger spread of thick sediments in our

Kirschbaum, 1995). Both our results clearly show a drop in sediment thickness to 0 km to the west nearing for the Black Hills region, a Cenozoic isolated mountain range with outcropping granite, pegmatite, and gneiss (Dahl *et al.*, 1999).

The inferred sediment thickness beneath the Rocky Mountains overall is very shallow, as expected, but to the east of the Rocky Mountain Front, the thick sediments generally correlate to the Western Interior Seaway as mentioned earlier, with a few exceptions (Fig. 4). Interestingly, our results show stations with thin (~1 km) sediments correspond to regions that have outcropped basement as mapped by Marshak *et al.* (2016).

MK10 show a generally thicker Wyoming basin (~6 km) in the Rocky Mountains than our predicted thickness (~3 km), similar to the depth to the basement from Marshak *et al.* (2016). This is despite the tomographic model showing a significant slow anomaly (Fig. 1b) and moderate delay times (Fig. 3). Notably, MK10 find thicker sediments in this region than in the Interior Plains to the east, whereas in our results the Interior Plains have thicker sediments. It is possible that the pick on the RFs in this area is a result of an intrabasin interface, rather than the true base of the sediments. There are indeed overlapping sediment basins of varying ages in this area (Coleman Jr and Cahan, 2012), and in the case of some higher-velocity intra-basin sedimentary packages (Mavko *et al.*, 2009), or where older sediments have metamorphosed, this could cause a significant impedance contrast between two sedimentary basins and bias the RF measurement (Marignier *et al.*, 2024).

The original data set of RFs from EarthScope automated receiver survey (Crotwell and Owens, 2005) unfortunately lacks much data in the interior of the Central Valley, California, or even within the greater Los Angeles region despite the large number of permanent and Transportable Array stations. However, with the addition of our new RFs, we can place some constraints on the deep basin structure in this area, such as station CI.VOG (Fig. 2). MK10 show a basin that is deeper at its western edge, but this is difficult to confirm with our available data. There are a few stations within the deep Los Angeles basin that confirm the >6- km-thick sedimentary package. The sediment thickness estimates for much of the West Coast are 0–2 km, but there is a lot of heterogeneity within the Cascadia subduction zone in northern California, Oregon, and Washington.

Conclusions

We have used a conceptually simple approach based on teleseismic RFs to create a new, consistent sediment thickness map across the conterminous United States. Using the time of seismic waves converted from P to S at what we interpret as the basement-sediment interface obtained from teleseismic P RFs, in combination with shear velocities from a tomographic model (Shen and Ritzwoller, 2016) and an empirical relationship (Marignier *et al.*, 2024), we obtain a detailed map of sediment thickness at the locations of over 1800 seismic stations. The

distribution of thick sediments is well correlated with known geological boundaries, with a few exceptions that can generally be understood by known limitations of the RF approach. This new sediment thickness map can be used for future tomographic studies of the United States by providing strong constraints on the shallowest sedimentary rock layer, as well as informing future estimates of national seismic hazard.

Data and Resources

The receiver function (RF) data used in this study were obtained from the EarthScope Automated Receiver Survey (Incorporated Research Institutions for Seismology Data Management Center [IRIS DMC], 2010, <https://ds.iris.edu/ds/products/cars/>, last accessed April 2024), maintained by the IRIS DMC Data Product efforts (Trabant *et al.*, 2012). The authors used the networks Transportable Array (TA) (IRIS Transportable Array, 2003), CI (California Institute of Technology and U.S. Geological Survey [USGS] Pasadena, 1926), BK (Northern California Earthquake Data Center, 2014), US (Albuquerque Seismological Laboratory [ASL]/USGS, 1990), and AZ (Vernon, 1982). Physiographic boundaries of the United States are from Fenneman and Johnson (1946). The tomographic model of Shen and Ritzwoller (2016) is available from IRIS EMC (2011). The sediment thickness map from MK10 was obtained from the central eastern United States—Seismic Source Characterization for Nuclear Facilities Project website (Central and Eastern United States Seismic Source Characterization [CEUS-SSC], 2012). The final data set of delay times and both sediment thickness estimates at all stations is available at Marignier (2024, <https://zenodo.org/records/14429658>). The supplemental material includes additional figures as described in the text.

Declaration of Competing Interests

The authors acknowledge that there are no conflicts of interest recorded.

References

- Abrahamson, N. A., W. J. Silva, and R. Kamai (2014). Summary of the ASK14 ground motion relation for active crustal regions, *Earthq. Spectra* **30**, no. 3, 1025–1055.
- Agrawal, S., C. M. Eakin, and J. O'Donnell (2022). Characterizing the cover across South Australia: A simple passive-seismic method for estimating sedimentary thickness, *Geophys. J. Int.* **231**, no. 3, 1850–1864.
- Albuquerque Seismological Laboratory (ASL)/USGS (1990). *United States national seismic network* [Dataset], doi: [10.7914/SN/US](https://doi.org/10.7914/SN/US).
- Berg, E. M., F.-C. Lin, V. Schulte-Pelkum, A. Allam, H. Qiu, and K. Gkogkas (2021). Shallow crustal shear velocity and V_p/V_s across southern California: Joint inversion of short-period Rayleigh wave ellipticity, phase velocity, and teleseismic receiver functions, *Geophys. Res. Lett.* **48**, no. 15, e2021GL092626, doi: [10.1029/2021GL092626](https://doi.org/10.1029/2021GL092626).
- Boore, D. M., J. P. Stewart, E. Seyhan, and G. M. Atkinson (2014). NGA-West2 equations for predicting PGA, PGV, and 5% damped PSA for shallow crustal earthquakes, *Earthq. Spectra* **30**, no. 3, 1057–1085.
- Boyd, O. S., D. Churchwell, M. P. Moschetti, E. M. Thompson, M. C. Chapman, O. Ilhan, T. L. Pratt, S. K. Ahdi, and S. Rezaeian (2024).

- Sediment thickness map of united states Atlantic and gulf coastal plain strata, and their influence on earthquake ground motions, *Earthq. Spectra* **40**, no. 1, 89–112.
- Brocher, T. M. (2005). Empirical relations between elastic wavespeeds and density in the earth's crust, *Bull. Seismol. Soc. Am.* **95**, no. 6, 2081–2092.
- California Institute of Technology and U.S. Geological Survey (USGS) Pasadena (1926). *Southern California Seismic Network* [Dataset], doi: [10.7914/SN/CI](https://doi.org/10.7914/SN/CI).
- Campbell, K. W., and Y. Bozorgnia (2014). Nga-west2 ground motion model for the average horizontal components of PGA, PGV, and 5% damped linear acceleration response spectra, *Earthq. Spectra* **30**, no. 3, 1087–1115.
- Central and Eastern United States Seismic Source Characterization (CEUS-SSC) (2012). *Central and Eastern United States Seismic Source Characterization for Nuclear Facilities* [Dataset], EPRI Technical Report, U.S. DOE, and U.S. NRC, Palo Alto, California, available at https://ceus-ssc.epri.com/GIS_Database (last accessed May 2024).
- Chai, C., C. J. Ammon, M. Maceira, and R. Herrmann (2022). Crust and upper mantle structure beneath the eastern united states, *Geochem. Geophys. Geosys.* **23**, no. 3, e2021GC010233, doi: [10.1029/2021GC010233](https://doi.org/10.1029/2021GC010233).
- Chai, C., C. J. Ammon, M. Maceira, and R. B. Herrmann (2015). Inverting interpolated receiver functions with surface wave dispersion and gravity: Application to the western U.S. and adjacent Canada and Mexico, *Geophys. Res. Lett.* **42**, no. 11, 4359–4366.
- Chichester, B., C. Rychert, N. Harmon, R. Allen, J. Collier, T. Henstock, and A. Rietbrock (2020). Seafloor sediment thickness beneath the voila broad-band ocean-bottom seismometer deployment in the lesser Antilles from p-to-s delay times, *Geophys. J. Int.* **223**, no. 3, 1758–1768.
- Coleman, J. L., Jr, and S. M. Cahan (2012). Preliminary catalog of the sedimentary basins of the united states, *U.S. Geol. Surv. Open-File Rept. 2012-1111*.
- Crotwell, H. P., and T. J. Owens (2005). Automated receiver function processing, *Seismol. Res. Lett.* **76**, no. 6, 702–709.
- Cunningham, E., and V. Lekic (2020). Constraining properties of sedimentary strata using receiver functions: An example from the Atlantic coastal plain of the southeastern United States, *Bull. Seismol. Soc. Am.* **110**, no. 2, 519–533.
- Dahl, P. S., D. K. Holm, E. T. Gardner, F. A. Hubacher, and K. A. Foland (1999). New constraints on the timing of early Proterozoic tectonism in the Black Hills (South Dakota), with implications for docking of the Wyoming province with Laurentia, *GSA Bull.* **111**, no. 9, 1335–1349.
- Deng, Y., Z. Li, S. Huang, Y. Xu, T. Hao, F. Bao, S. Zhang, S. Li, X. Jia, P. Tian, et al. (2023). Structure of the Gonghe sedimentary basin in the northeastern Tibetan plateau: Evidence from teleseismic *P*-waves recorded by a dense seismic array, *Geophys. J. Int.* **235**, 1697–1711.
- Domrois, S. L., S. Marshak, C. C. Abert, and T. H. Larson (2015). ArcGIS maps depicting topography of the basement-cover contact (the great unconformity), and the traces of faults and folds, in the Cratonic platform of the United States, American Association of Petroleum Geologists Search and Discovery, 29 pp., available at https://www.searchanddiscovery.com/pdfz/documents/2015/30410domrois/ndx_domrois.pdf.html (last accessed September 2024).
- Ekström, G. (2014). Love and Rayleigh phase-velocity maps, 5–40 s, of the western and central USA from USArray data, *Earth Planet. Sci. Lett.* **402**, 42–49.
- Ettensohn, F. R. (2008). Chapter 4 The Appalachian Foreland basin in eastern United States, in *Sedimentary Basins of the World*, A. D. Miall (Editor), Vol. 5, Elsevier, 105–179.
- Fenneman, N., and D. Johnson (1946). Physiographic divisions of the conterminous U.S., *U.S. Geol. Surv. Data Release*, available at <https://www.sciencebase.gov/catalog/item/631405bbd34e36012efa304e> (last accessed May 2024).
- Frezon, S. E., T. Finn, and J. M. Lister (1983). Total thickness of sedimentary rocks in the conterminous United States, *U.S. Geol. Surv. Open-File Rept. 83-920*.
- Ghose, R., P. Persaud, and R. W. Clayton (2023). Basin structure for earthquake ground motion estimates in urban Los Angeles mapped with nodal receiver functions, *Geosciences* **13**, no. 11, 320.
- Incorporated Research Institutions for Seismology Data Management Center (IRIS DMC) (2010). *Data services products: EARS EarthScope automated receiver survey* [Dataset], available at <https://ds.iris.edu/ds/products/ears/> (last accessed April 2024).
- IRIS EMC (2011). *Data services products: EMC, A repository of Earth models* [Dataset], doi: [10.17611/DP/EMC.1](https://doi.org/10.17611/DP/EMC.1).
- IRIS Transportable Array (2003). *USArray transportable array* [Dataset], International Federation of Digital Seismograph Networks, doi: [10.7914/SN/TA](https://doi.org/10.7914/SN/TA).
- Kim, H., H. Kawakatsu, T. Akuhara, and N. Takeuchi (2023). Characterizing the seafloor sediment layer using teleseismic body waves recorded by ocean bottom seismometers, *J. Geophys. Res.* **128**, no. 12, e2023JB027616, doi: [10.1029/2023JB027616](https://doi.org/10.1029/2023JB027616).
- Laske, G. (1997). A global digital map of sediment thickness, *Eos Trans. AGU* **78**, F483.
- Laske, G., G. Masters, Z. Ma, and M. Pasynos (2012). CRUST1.0: An updated global model of Earth's crust, *EGU General Assembly 2012, Geophysical Research Abstracts*, Vol. 14, 743.
- Levander, A., and M. S. Miller (2012). Evolutionary aspects of lithosphere discontinuity structure in the western U.S., *Geochem. Geophys. Geosys.* **13**, no. 7, doi: [10.1029/2012GC004056](https://doi.org/10.1029/2012GC004056).
- Li, G., T. S. Bidgoli, M. Chen, X. Ma, and J. Li (2022). Sedimentary and crustal structure of the western united states from joint inversion of multiple passive seismic datasets, *J. Geophys. Res.* **127**, no. 2, e2021JB022384, doi: [10.1029/2021JB022384](https://doi.org/10.1029/2021JB022384).
- Lin, F.-C., M. P. Moschetti, and M. H. Ritzwoller (2008). Surface wave tomography of the western united states from ambient seismic noise: Rayleigh and love wave phase velocity maps, *Geophys. J. Int.* **173**, no. 1, 281–298.
- Liu, G., P. Persaud, and R. W. Clayton (2018). Structure of the northern Los Angeles basins revealed in teleseismic receiver functions from short-term nodal seismic arrays, *Seismol. Res. Lett.* **89**, no. 5, 1680–1689.
- Liu, K., A. Levander, F. Niu, and M. S. Miller (2011). Imaging crustal and upper mantle structure beneath the Colorado Plateau using finite frequency Rayleigh wave tomography, *Geochem. Geophys. Geosys.* **12**, no. 7, doi: [10.1029/2011GC003611](https://doi.org/10.1029/2011GC003611).

- Marignier, A. (2024). *Sediment thickness of the USA from seismic receiver functions (v2.0)* [Dataset], available at <https://zenodo.org/records/14429658> (last accessed December 2024).
- Marignier, A., C. M. Eakin, B. Hejrani, S. Agrawal, and R. Hassan (2024). Sediment thickness across Australia from passive seismic methods, *Geophys. J. Int.* **237**, no. 2, 849–861.
- Marshak, S., S. Domrois, C. Abert, and T. Larson (2016). *DEM of the great unconformity, USA cratonic platform* [Dataset], available at <https://databank.illinois.edu/datasets/IDB-7546972> (last accessed September 2024).
- Mavko, G., T. Mukerji, and J. Dvorkin (2009). *The Rock Physics Handbook: Tools for Seismic Analysis of Porous Media*, Second Ed., Cambridge University Press, Cambridge, United Kingdom.
- Miall, A. D., O. Catuneanu, B. K. Vakarelov, and R. Post (2008). Chapter 9 The western interior basin, in *Sedimentary Basins of the World*, A. D. Miall (Editor), Vol. 5, Elsevier, Amsterdam, the Netherlands, 329–362.
- Molnar, S., J. F. Cassidy, K. B. Olsen, S. E. Dosso, and J. He (2014). Earthquake ground motion and 3D Georgia basin amplification in southwest British Columbia: Shallow blind-thrust scenario earthquakes, *Bull. Seismol. Soc. Am.* **104**, no. 1, 321–335.
- Mooney, W. D., and M. K. Kaban (2010). The North American upper mantle: Density, composition, and evolution, *J. Geophys. Res.* **115**, no. B12, doi: [10.1029/2010JB000866](https://doi.org/10.1029/2010JB000866).
- Moschetti, M. P., M. H. Ritzwoller, and N. M. Shapiro (2007). Surface wave tomography of the western united states from ambient seismic noise: Rayleigh wave group velocity maps, *Geochem. Geophys. Geosys.* **8**, no. 8, doi: [10.1029/2007GC001655](https://doi.org/10.1029/2007GC001655).
- Northern California Earthquake Data Center (2014). *Berkeley Digital Seismic Network (BDSN)* [Dataset], doi: [10.7932/BDSN](https://doi.org/10.7932/BDSN).
- Petersen, M. D., A. M. Shumway, P. M. Powers, C. S. Mueller, M. P. Moschetti, A. D. Frankel, S. Rezaeian, D. E. McNamara, N. Luco, et al. (2020). The 2018 update of the U.S. National Seismic Hazard Model: Overview of model and implications, *Earthq. Spectra* **36**, no. 1, 5–41.
- Roberts, L. N. R., and M. A. Kirschbaum (1995). Paleogeography and the Late Cretaceous of the Western Interior of middle North America; coal distribution and sediment accumulation, *Rept. 1561*, doi: [10.3133/pp1561](https://doi.org/10.3133/pp1561).
- Sadler, B., and J. Pulliam (2023). Modeling crustal structure in the Permian basin by waveform-matching p receiver functions and autocorrelograms with particle swarm optimization, *J. Geophys. Res.* **128**, no. 6, e2023JB026730, doi: [10.1029/2023JB026730](https://doi.org/10.1029/2023JB026730).
- Sadler, B., and J. Pulliam (2025). Probing complex crustal structure across the south-central united states using receiver functions and autocorrelograms, *J. Geophys. Res.* **130**, no. 2, e2024JB030064, doi: [10.1029/2024JB030064](https://doi.org/10.1029/2024JB030064).
- Schmandt, B., F.-C. Lin, and K. E. Karlstrom (2015). Distinct crustal isostasy trends east and west of the rocky mountain front, *Geophys. Res. Lett.* **42**, no. 23, 10,290–10,298.
- Shen, W., and M. H. Ritzwoller (2016). Crustal and uppermost mantle structure beneath the United States, *J. Geophys. Res.* **121**, no. 6, 4306–4342.
- Shen, W., M. H. Ritzwoller, and V. Schulte-Pelkum (2013). Crustal and uppermost mantle structure in the central U.S. encompassing the midcontinent rift, *J. Geophys. Res.* **118**, no. 8, 4325–4344.
- Shen, W., M. H. Ritzwoller, V. Schulte-Pelkum, and F.-C. Lin (2012). Joint inversion of surface wave dispersion and receiver functions: A Bayesian Monte-Carlo approach, *Geophys. J. Int.* **192**, no. 2, 807–836.
- Sturgeon, W., A. M. G. Ferreira, L. Schardong, and A. Marignier (2023). Crustal structure of the western U.S. from Rayleigh and love wave amplification data, *J. Geophys. Res.* **128**, no. 8, e2022JB026148, doi: [10.1029/2022JB026148](https://doi.org/10.1029/2022JB026148).
- Trabant, C., A. R. Hutko, M. Bahavar, R. Karstens, T. Ahern, and R. Aster (2012). Data products at the iris DMC: Stepping stones for research and other applications, *Seismol. Res. Lett.* **83**, no. 5, 846–854.
- Vernon, F. (1982). *ANZA regional network* [Dataset], doi: [10.7914/SN/AZ](https://doi.org/10.7914/SN/AZ).
- Wang, X., Z. Zhan, M. Zhong, P. Persaud, and R. W. Clayton (2021). Urban basin structure imaging based on dense arrays and Bayesian array-based coherent receiver functions, *J. Geophys. Res.* **126**, no. 9, e2021JB022279, doi: [10.1029/2021JB022279](https://doi.org/10.1029/2021JB022279).
- Whitmeyer, S. J., and K. E. Karlstrom (2007). Tectonic model for the Proterozoic growth of North America, *Geosphere* **3**, no. 4, 220–259.
- Wirth, E. A., J. E. Vidale, A. D. Frankel, T. L. Pratt, N. A. Marafi, M. Thompson, and W. J. Stephenson (2019). Source-dependent amplification of earthquake ground motions in deep sedimentary basins, *Geophys. Res. Lett.* **46**, no. 12, 6443–6450.
- Yang, X., G. L. Pavlis, M. W. Hamburger, S. Marshak, H. Gilbert, J. Rupp, T. H. Larson, C. Chen, and N. S. Carpenter (2017). Detailed crustal thickness variations beneath the Illinois basin area: Implications for crustal evolution of the midcontinent, *J. Geophys. Res.* **122**, no. 8, 6323–6345.
- Yeck, W. L., A. F. Sheehan, and V. Schulte-Pelkum (2013). Sequential $H - \kappa$ stacking to obtain accurate crustal thicknesses beneath sedimentary basins, *Bull. Seismol. Soc. Am.* **103**, no. 3, 2142–2150.

Manuscript received 1 March 2025
Published online 9 June 2025